

Supporting Information of

Time Resolved EPR Characterization of a Folded Conformation of Photoinduced Charge-Separated State in Fullerene-Porphyrin Dyad Bridged by Diphenyldisilane

Yasuhiro Kobori,^{*,†} Yuki Shibano,^{‡,§} Tsubasa Endo,[†] Hayato Tsuji,^{‡,¶} Hisao Murai,[†] and Kohei Tamao^{‡,⊥}

Contribution from Department of Chemistry, Faculty of Science, Shizuoka University, 836 Ohya Surugaku, Shizuoka 422-8529 Japan, Institute for Chemical Research, Kyoto University Uji, 611-0011 Kyoto, Japan

1. Experimental

Samples. Benzonitrile (> 98 %, Wako) was used as received. The fullerene-porphyrin dyad (ZnP-C₆₀) linked with diphenyldisilane bridge was synthesized as reported previously.¹ For the TREPR measurement, the concentration of ZnP-C₆₀ was 2×10^{-4} M.

UV-Visible Spectroscopy.

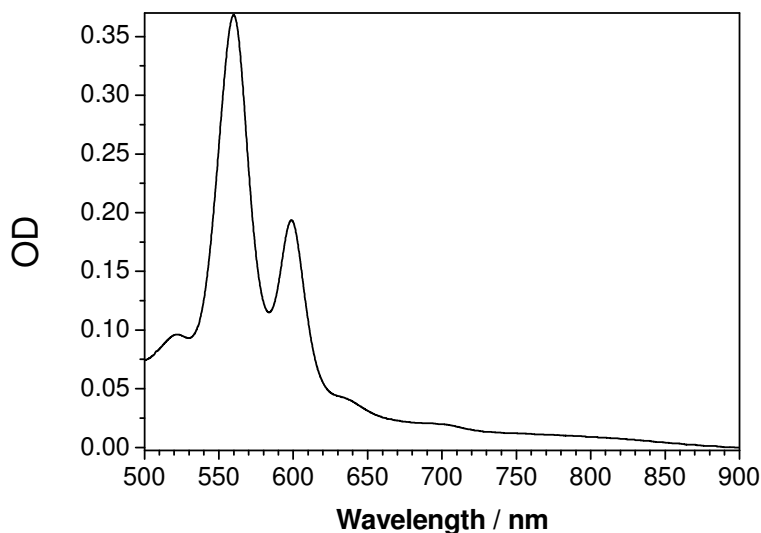


Figure S1. Steady-state absorption spectrum of ZnP-C₆₀ (2×10^{-4} M) of the present system in benzonitrile at room temperature. This spectrum is very similar to the absorption spectrum of the ZnP-C₆₀ dyad (ZnP-Si₅-C₆₀) bridged by pentasilane. As is reported for the ZnP-Si₅-C₆₀, a broad absorption band is observed in this system at the near infrared region (from 620 nm to 900 nm) which is characteristic of molecules that have an interaction between the ZnP and C₆₀ moieties. This result supports that their exist at least two folded molecular structures with the large and the small π -orbital overlaps those of which are optically-detected and EPR conformations, respectively. (See text.)

Time-resolved EPR. The X-band TREPR measurements were carried out using a Bruker EMX system. In the microwave bridge, a modified preamplifier (ER047PH) in which the time resolution is enhanced (~60 ns) was equipped. Light excitations were performed by the second harmonic (532 nm) of a Nd:YAG laser (Continuum, Minilite II, fwhm ~5 ns). Transient signals were averaged by a digital oscilloscope (Tektronix, TDS 520D) at 201 different external magnetic field positions and were transferred to a personal computer via a GPIB communication to obtain the 2-dimensional TREPR data. Temperature was controlled by a nitrogen-gas flow system. The nitrogen gas was flowed through a liquid-nitrogen container and was transferred to a sample dewar inserted in a microwave cavity. Temperature was controlled by the flow rate of the nitrogen gas.

2. Analysis of the TREPR spectra

2.1 Computation of the electron spin polarization by the ESPT from the excited triplet state to the CS state.

According to Scheme 1 in the manuscript, the eigenfunctions (T_l , T_m and T_n in Scheme 1) under the applied magnetic field in $\text{ZnP-}^3\text{C}_{60}^*$ can be obtained by the following relations.

$$\begin{pmatrix} |T_l\rangle \\ |T_m\rangle \\ |T_n\rangle \end{pmatrix} = \mathbf{U}^T \begin{pmatrix} |T_x\rangle \\ |T_y\rangle \\ |T_z\rangle \end{pmatrix}, \quad (\text{S1})$$

where \mathbf{U} represents the matrix composed of the eigenvectors that diagonalize the spin Hamiltonian \mathbf{H}_T of the excited triplet state of $^3\text{C}_{60}^*$ under the applied magnetic field B_0 so that the diagonal matrix of $\boldsymbol{\varepsilon}$ composed of the eigenvalues ε_l , ε_m and ε_n is represented as $\boldsymbol{\varepsilon} = \mathbf{U}^{-1}\mathbf{H}_T\mathbf{U}$. The population $\boldsymbol{\rho}_T$ of the T_l , T_m and T_n levels in Scheme 1 can be obtained as follows,

$$\boldsymbol{\rho}_T = \mathbf{U}^{-1} \boldsymbol{\rho}_{XYZ} \mathbf{U}, \quad (\text{S2})$$

where $\boldsymbol{\rho}_{XYZ}$ denotes the population for the zero-field donor sublevels in a molecular frame by the S_1 - T_1 intersystem crossing represented as follows,

$$\boldsymbol{\rho}_{XYZ} = \begin{pmatrix} p_X & & \\ & p_Y & \\ & & p_Z \end{pmatrix}, \quad (\text{S3})$$

with $p_X + p_Y + p_Z = 1$. In eq. (S2), it is noted that the off-diagonal terms in $\boldsymbol{\rho}_T$ can be set to zero when the lifetime ($\sim 0.3 \mu\text{s}$ for $\text{ZnP-}^3\text{C}_{60}^*$ in the present study) of the donor triplet state is much longer than the phase memory time ($T_2 < 10 \text{ ns}$ in typical excited triplet EPR spectra) under the external magnetic field; i.e. $\boldsymbol{\rho}_T(T_l, T_m) = \boldsymbol{\rho}_T(T_l, T_n) = \boldsymbol{\rho}_T(T_m, T_l) = \boldsymbol{\rho}_T(T_m, T_n) = \boldsymbol{\rho}_T(T_n, T_l) = \boldsymbol{\rho}_T(T_n, T_m) = 0$ in eq.(S2).

When the hyperfine coupling is negligibly smaller than the spin dipolar interaction in the CS state, the eigenfunctions (T_+ , T_0 and T_- in Scheme 1) under the applied magnetic field in the CS state ($\text{ZnP}^+-\text{C}_{60}^-$) can be obtained by the following relations using basis wavefunctions (T_x' , T_y' and T_z') that diagonalize the dipolar interaction of the RP at the zero-field.

$$\begin{pmatrix} |T_+\rangle \\ |T_0\rangle \\ |T_-\rangle \end{pmatrix} = \mathbf{V}^T \begin{pmatrix} |T_x'\rangle \\ |T_y'\rangle \\ |T_z'\rangle \end{pmatrix}, \quad (\text{S4})$$

where V represents the matrix composed of the eigenvectors that diagonalize the spin Hamiltonian H_{RP} (vide infra) of the triplet CS state under the applied magnetic field B_0 .

During the charge separation process, the characters of the T_X , T_Y and T_Z wavefunctions in the excited triplet are conserved in the T_+ , T_0 and T_- wavefunctions of the triplet CS states. The probability of finding the T_i ($i = X, Y$ and Z) character in the T_j ($j = X', Y'$ and Z') is represented as $\langle T_i | T_j \rangle^2 = \cos^2 \theta_{ij}$ where θ_{ij} is the angle between the principal axis of the excited triplet state and the principal axis of the CS state. Thus, the population ρ_{RP} of the T_+ , T_0 and T_- levels created by the ESPT from the excited triplet state to the CS state can be obtained as follows,²

$$\rho_{RP,k'} = \sum_k \sum_i \sum_j |U(i,k)|^2 |V(j,k')|^2 \langle T_i | T_j \rangle^2 \rho_T(T_k, T_k), \quad (S5)$$

where k' ($= +, 0,$ and $-$) specifies T_+ , T_0 and T_- in the CS state under the applied magnetic field in Scheme 1. When the CS state undergoes the S- T_0 mixing to create the spin-correlated RP, the four eigenstates are obtained as,³ $|\mathbf{a}\rangle = |\mathbf{T}_+\rangle$, $|\mathbf{b}\rangle = \cos\mu |\mathbf{S}\rangle + \sin\mu |\mathbf{T}_0\rangle$, $|\mathbf{c}\rangle = -\sin\mu |\mathbf{S}\rangle + \cos\mu |\mathbf{T}_0\rangle$ and $|\mathbf{d}\rangle = |\mathbf{T}_-\rangle$, where the spin Hamiltonian H_{RP} composed of Zeeman interaction, the dipolar interaction and the hyperfine interaction is diagonalized under the high B_0 limit. From eq. (S5), the initial populations of the CS state (ρ_{aa}^0 , ρ_{bb}^0 , ρ_{cc}^0 and ρ_{dd}^0) in $|\mathbf{a}\rangle$, $|\mathbf{b}\rangle$, $|\mathbf{c}\rangle$ and $|\mathbf{d}\rangle$ can be computed as,

$$\rho_{aa}^0 = \rho_{RP,+}, \quad (S6)$$

$$\rho_{bb}^0 = \rho_{RP,0} \cdot \sin^2 \mu, \quad (S7)$$

$$\rho_{cc}^0 = \rho_{RP,0} \cdot \cos^2 \mu, \quad (S8)$$

$$\rho_{dd}^0 = \rho_{RP,-}. \quad (S9)$$

Here, the angle μ is related as follows,⁴

$$\cos \mu = \frac{2Q_-}{\sqrt{2\omega_2(\omega_2 - 2J - 2d)}}, \quad \sin \mu = \sqrt{\frac{\omega_2 - 2J - 2d}{2\omega_2}} \quad (S10)$$

with $\omega_2 = [(2J + 2d)^2 + 4Q_-^2]^{1/2}$, where Q_- denotes the Lamor frequency difference between ZnP^{+} and $C60^-$ and is represented using the g factors and hyperfine coupling constants (a) as,

$$Q_- = \frac{1}{2} \left\{ (g_{ZnP,eff} - g_{C60,eff}) \beta B_0 + \sum_m a_{ZnP,m} M_{ZnP,m} - \sum_n a_{C60,m} M_{C60,m} \right\}. \quad (S11)$$

2.2 Time dependence of the spin-state populations.

In the limit of the fast spin-spin relaxation in the zero-quantum coherences for the off-diagonal terms (ρ_{bc} and ρ_{cb}), the time-evolution of the SCRPs (ρ_{kk}) simplifies to a set of coupled time-differential equations⁵ in ρ_{abcd}

$$\begin{pmatrix} \dot{\rho}_{aa} \\ \dot{\rho}_{bb} \\ \dot{\rho}_{cc} \\ \dot{\rho}_{dd} \end{pmatrix} = \begin{pmatrix} -w_{ab} - w_{ac} & w_{ba} & w_{ca} & 0 \\ w_{ab} & -w_{ba} - w_{bc} - w_{bd} - k_{CR2} \cos^2 \mu & w_{cb} & w_{db} \\ w_{ac} & w_{bc} & -w_{ca} - w_{cb} - w_{cd} - k_{CR2} \sin^2 \mu & w_{dc} \\ 0 & w_{bd} & w_{cd} & -w_{db} - w_{dc} \end{pmatrix} \begin{pmatrix} \rho_{aa} \\ \rho_{bb} \\ \rho_{cc} \\ \rho_{dd} \end{pmatrix} \quad (\text{S12})$$

where w_{ij} denotes the spin-lattice relaxation rate constant between the i and j states in $|a\rangle$, $|b\rangle$, $|c\rangle$ and $|d\rangle$. The relaxation rate constants can be related as follows,

$$w_{ac} = w_{ca} \exp\left(\frac{\hbar\nu_{MW}}{k_B T}\right), \quad w_{bd} = w_{db} \exp\left(\frac{\hbar\nu_{MW}}{k_B T}\right), \quad w_{ab} = w_{ba} \exp\left(\frac{\hbar\nu_{MW}}{k_B T}\right), \quad w_{cd} = w_{dc} \exp\left(\frac{\hbar\nu_{MW}}{k_B T}\right), \quad (\text{S13})$$

where ν_{MW} denotes the microwave frequency (= 9.4 GHz in the present study). In this study, $w_{ac} = w_{bd} = w_{ab} = w_{cd}$ and $w_{ca} = w_{db} = w_{ba} = w_{dc}$ are assumed and a single spin lattice relaxation time ($T_1 = 10 \mu\text{s}$) was set as follows,

$$T_1 = \frac{1}{w_{ac} + w_{ca}} = \frac{1}{w_{ab} + w_{ba}} = \frac{1}{w_{bd} + w_{db}} = \frac{1}{w_{cd} + w_{dc}} \quad (\text{S14})$$

The relaxation times ($T_{bc} = 1/w_{bc} = 1/w_{cb}$) between $|b\rangle$ and $|c\rangle$ states correspond to the dephasing time between the S and T_0 states induced by fluctuations of the exchange and dipolar interactions.⁶ $T_{bc} = 3.0 \mu\text{s}$ was considered as described in the manuscript. The sublevel-selective spin relaxation between $|b\rangle$ and $|c\rangle$ states is very consistent with the small exchange interaction obtained in this study.

Time-evolution of the matrix of ρ_{abcd} composed of ρ_{aa} , ρ_{bb} , ρ_{cc} and ρ_{dd} in eq. (S12) was calculated by solving eq. (S12) as $\rho_{abcd}(t) = \mathbf{S} \cdot \exp(\boldsymbol{\eta}t) \cdot \mathbf{S}^{-1} \cdot \rho_{abcd}(t=0)$ where \mathbf{S} and $\boldsymbol{\eta}$ are the matrices of eigenvectors and eigenvalues of the relaxation matrix in eq. (S12). $\rho_{abcd}(t=0)$ denotes initial populations in eqs. (S6)-(S9). For the EPR transitions among the four levels, the transition intensities are represented as,³ $I_{ab}(t) = [\rho_{bb}(t) - \rho_{aa}(t)]\sin^2\mu$, $I_{ac}(t) = [\rho_{cc}(t) - \rho_{aa}(t)]\cos^2\mu$, $I_{bd}(t) = [\rho_{dd}(t) - \rho_{bb}(t)]\sin^2\mu$ and $I_{cd}(t) = [\rho_{dd}(t) - \rho_{cc}(t)]\cos^2\mu$. $\rho_{abcd}(t)$ and were used for the computations of the TREPR spectrum.

2.3 Angle settings.

In the molecular frame (X' , Y' and Z') of the zero-field splitting interaction, the spin Hamiltonian of the triplet CS state is expressed as follows,

$$\hat{H}_{RP}(\Omega) = g\beta B_0(\Omega)\hat{S} - X'\hat{S}_X^2 - Y'\hat{S}_Y^2 - Z'\hat{S}_Z^2 + \sum_m a_{ZnP,m}\hat{S}_1\hat{I}_{ZnP,m} + \sum_n a_{C60,m}\hat{S}_2\hat{I}_{C60,m} - 2J(1/2 + \hat{S}_1\hat{S}_2), \quad (S14)$$

where g represents the effective g value in the CS state and is assumed to be isotropic since the D anisotropy is much larger than the anisotropy in the g factor in this system. On the basis of the T_X' , T_Y' and T_Z' functions, eq. (S14) is expressed as follows under the high-field approximation. ($g\beta B_0 \gg |a_i|$)

$$\hat{H}_{RP}(\Omega) = \begin{pmatrix} \langle T_X' | \\ \langle T_Y' | \\ \langle T_Z' | \end{pmatrix} \begin{pmatrix} D/3 - J & -ig\beta B_0 \cos \theta_B & ig\beta B_0 \sin \phi_B \sin \theta_B \\ ig\beta B_0 \cos \theta_B & D/3 - J & -ig\beta B_0 \cos \phi_B \sin \theta_B \\ -ig\beta B_0 \sin \phi_B \sin \theta_B & ig\beta B_0 \cos \phi_B \sin \theta_B & -2D/3 - J \end{pmatrix}, \quad (S15)$$

where θ_B and ϕ_B are the polar angles of the external magnetic field B_0 with respect to the Z' and X' principal axes, respectively, in the zero-field splitting interaction of the CS state. \mathbf{V} in eq. (S4) was obtained as the eigenvectors that diagonalize the spin Hamiltonian \mathbf{H}_{RP} of eq. (S15).

In the CS state, the energy levels have been approximated under the high-field limit as follows,⁴

$$\begin{aligned} \omega_a &= Q_+ + d - J \\ \omega_b &= -d + \frac{\omega_2}{2} \\ \omega_c &= -d - \frac{\omega_2}{2} \\ \omega_d &= -Q_+ + d - J \end{aligned} \quad (S16)$$

where

$$Q_+ = \frac{1}{2} \left\{ (g_{ZnP,eff} + g_{C60,eff})\beta B_0 + \sum_m a_{ZnP,m}M_{ZnP,m} + \sum_n a_{C60,m}M_{C60,m} \right\}, \quad (S17)$$

with

$$d = \frac{D}{2} \left(\cos^2 \theta_B - \frac{1}{3} \right) \quad (S18)$$

In ZnP^+ , hyperfine couplings ($a_N = 0.22$ mT)⁵ from the four nitrogen atoms were considered in the CS state. In $C60^-$, the hyperfine coupling is negligibly small.

In the XYZ coordinate system of the excited triplet molecule, the magnetic field \mathbf{B}_0 can be expressed using the angles of θ , ϕ , θ_B and ϕ_B as follows,

$$\begin{pmatrix} B_X \\ B_Y \\ B_Z \end{pmatrix} = B_0 \begin{pmatrix} \sin \phi & \cos \theta \cos \phi & \sin \theta \cos \phi \\ -\cos \phi & \cos \theta \sin \phi & \sin \theta \sin \phi \\ 0 & -\sin \theta & \cos \theta \end{pmatrix} \begin{pmatrix} \cos \phi_B \sin \theta_B \\ \sin \phi_B \sin \theta_B \\ \cos \theta_B \end{pmatrix}. \quad (\text{S19})$$

The spin Hamiltonian \mathbf{H}_T of the excited triplet state of ${}^3\text{C}_{60}^*$ is expressed as follows,

$$\hat{\mathbf{H}}_T(\boldsymbol{\Omega}) = \begin{pmatrix} \langle T_X | \\ \langle T_Y | \\ \langle T_Z | \end{pmatrix} \begin{pmatrix} X & -ig\beta B_Z & ig\beta B_Y \\ ig\beta B_Z & Y & -ig\beta B_X \\ -ig\beta B_Y & ig\beta B_X & Z \end{pmatrix}, \quad (\text{S20})$$

where $X = D_T/3 - E_T$, $Y = D_T/3 + E_T$, and $Z = -2D_T/3$. \mathbf{H}_T of the excited triplet state has been diagonalized to compute \mathbf{U} in eqs. (S1), (S2) and (S5).

In this study, the principal axes of the g tensors of the $\text{C}_{60}^{\cdot-}$ and ZnP^{+} were assumed to be collinear with the X, Y and Z axes. Thus the effective g values in eq. (S17) can be obtained as follows,

$$g_{i,eff} = \frac{\sqrt{g_{i,x}^2 B_X^2 + g_{i,y}^2 B_Y^2 + g_{i,z}^2 B_Z^2}}{B_0}. \quad (\text{S21})$$

$g_{\text{C}_{60},x} = 2.00085$, $g_{\text{C}_{60},y} = 2.00038$ and $g_{\text{C}_{60},z} = 1.99925$ were used from reported study.⁷ $g_{\text{ZnP},x} = 2.00265$, $g_{\text{ZnP},y} = 2.00265$ and $g_{\text{ZnP},z} = 2.0022$ were used as reported previously.⁸

In eq. (S5), direction cosines between the principal axes are represented from Figure 2b as follows,

$$\begin{aligned} \langle T_X | T_X \rangle^2 &= \sin^2 \phi, \quad \langle T_Y | T_X \rangle^2 = \cos^2 \phi, \quad \langle T_Z | T_X \rangle^2 = 0, \\ \langle T_X | T_Y \rangle^2 &= \cos^2 \theta \cos^2 \phi, \quad \langle T_Y | T_Y \rangle^2 = \cos^2 \theta \sin^2 \phi, \quad \langle T_Z | T_Y \rangle^2 = \sin^2 \theta, \\ \langle T_X | T_Z \rangle^2 &= \sin^2 \theta \cos^2 \phi, \quad \langle T_Y | T_Z \rangle^2 = \sin^2 \theta \sin^2 \phi, \quad \langle T_Z | T_Z \rangle^2 = \cos^2 \theta. \end{aligned} \quad (\text{S22})$$

The time-dependent EPR spectra were computed by summing the above four i - j transitions of \mathbf{a} - \mathbf{b} , \mathbf{a} - \mathbf{c} , \mathbf{b} - \mathbf{c} and \mathbf{b} - \mathbf{d} obtained at all possible equally distributed molecular orientations of $\boldsymbol{\Omega}$ with respect to the direction of \mathbf{B}_0 . The powder pattern $SP(t)$ of the EPR spectrum is thus represented by the sum of the Lorentzian shape functions as follows,

$$SP(t) = \int_0^{2\pi} \int_0^\pi \sum_{i,j} \text{Im} \frac{I_{ij}(t)}{\omega_i - \omega_j + \omega_0 - \frac{i}{T_2}} \sin \theta_B d\phi_B d\theta_B, \quad (\text{S23})$$

where ω_i denotes the energy levels in the unit of angular frequency of the \mathbf{a} , \mathbf{b} , \mathbf{c} and \mathbf{d} levels in the CS state. (eq. S16) ω_0 is the angular frequency of the microwave.

3. Assignments of the charge separated states

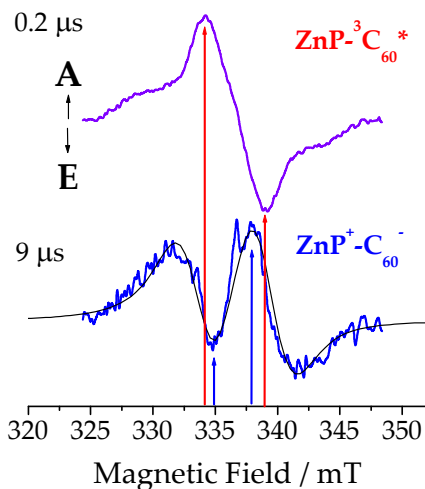


Figure S2. Comparison of the TREPR spectra at two time windows obtained by the photolysis of the ZnP-C₆₀. It is obvious that the peak positions (red arrows) at the early time are different from the positions (blue arrows) at the later time, indicating that the spectrum obtained at 9 μs is from different species from the excited triplet of ³C₆₀*. From the midpoint field value (336.565 mT) from the red arrows, $g_{av} = 2.0013$ was obtained. This is consistent with $g_{av} = 2.0014$ reported for the excited triplet state of fulleropyrrolidine molecule.⁷ The TREPR spectrum at 9 μs is also consistent with the simulation of the EPR spectrum for the charge-separated state calculated by the g-factors of C₆₀* and of ZnP*⁺ ($g_{C_{60,x}} = 2.00085$, $g_{C_{60,y}} = 2.00038$, $g_{C_{60,z}} = 1.99925$, $g_{ZnP,x} = 2.00265$, $g_{ZnP,y} = 2.00265$ and $g_{ZnP,z} = 2.0022$) as described above.

In the optically-detected folded conformation, the CS rate constant is reported to be $\sim 4 \times 10^9 \text{ s}^{-1}$ which was obtained from the fluorescence decays of the excited singlet states of ZnP in a frozen media.⁹ If the optically-detected conformations were detected by the TREPR measurement, quick rise components of the CS state should be seen. We did not see any signal contributions from the CS state at the early time region ($< 300 \text{ ns}$) as shown in Figure 2a, indicating that the optically-detected folded conformation is not detectable by the TREPR. By using the relation $2J = |V|^2/\Delta E$ as described in the manuscript, $2J = 5 \text{ T}$ is calculated as the singlet-triplet energy gap when $|V| = 200 \text{ cm}^{-1}$ is used as reported in an optically-detected CS state of a compact ZnP-C₆₀ system.¹⁰ Under this condition that the exchange coupling is extremely larger than the Zeeman energy, no EPR transition is possible for the optically-detected CS state because of the absence of the singlet-triplet mixing. Therefore, even when the singlet RP is created in the optically detected folded conformation, the CS state cannot be detected by the TREPR and is quickly deactivated due to the fast CR process through the singlet manifold. Above arguments strongly support that the EPR conformation obtained in this study is totally different from the

optically detected conformation and that, in the CS state of the EPR conformation, the SOMO-SOMO orbitals are orthogonal, as shown in Figure 2b.

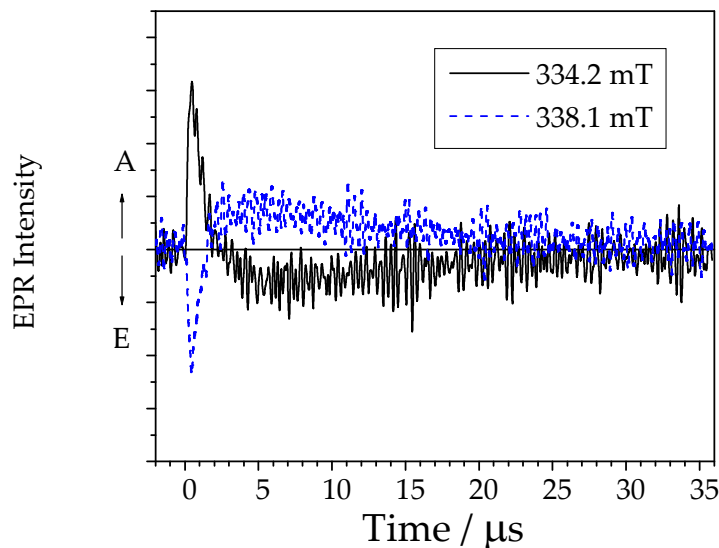


Figure S3. Time profiles of the TREPR signals at 334.1 and 338.1 mT. Initial quick decays ($> 10^6 \text{ s}^{-1}$) of the A/E signals are attributed to the decays of the $\text{ZnP-}^3\text{C}_{60}^*$ by the photoinduced CS. The rises of the initial CS state polarization (A/E) by the ESPT are hidden by the decays of to the $\text{ZnP-}^3\text{C}_{60}^*$ signals. The slower rises ($\sim 2 \times 10^5 \text{ s}^{-1}$) of the components of the E and the A signals are seen in this figure and are explained by the singlet CR reaction to create the correlated RP spin polarization with A/E/A/E pattern that is due to the S- T_0 mechanism. The slow decays ($\sim 1 \times 10^5 \text{ s}^{-1}$) of the signals are attributable to the spin-lattice relaxation ($T_1 = 10 \mu\text{s}$ as described in page 5) in the correlated RP. Since the singlet CR reaction is faster than the spin-lattice relaxation under the applied magnetic field, the decays of the CS state must be governed by the spin-lattice relaxation. Above data ambiguously support the kinetic data ($T_{bc} = 3.0 \mu\text{s}$ and $k_{CR} = 2.0 \times 10^5 \text{ s}^{-1}$) presented in the manuscript.

References

1. Sasaki, M.; Shibano, Y.; Tsuji, H.; Araki, Y.; Tamao, K.; Ito, O., *J. Phys. Chem. A* **2007**, *111*, 2973-2979.
2. Akiyama, K.; Tero-Kubota, S.; Ikoma, T.; Ikegami, Y., *J. Am. Chem. Soc.* **1994**, *116*, 5324-5327.
3. Closs, G. L.; Forbes, M. D. E.; Norris, J. R., *J. Phys. Chem.* **1987**, *91*, 3592-3599.
4. Morris, A. L.; Snyder, S. W.; Zhang, Y. N.; Tang, J.; Thurnauer, M. C.; Dutton, P. L.; Robertson, D. E.;

- Gunner, M. R., *J. Phys. Chem.* **1995**, *99*, 3854-3866.
5. Kobori, Y.; Yamauchi, S.; Akiyama, K.; Tero-Kubota, S.; Imahori, H.; Fukuzumi, S.; Norris, J. R., *Proc. Natl. Acad. Sci. U. S. A.* **2005**, *102*, 10017-10022.
6. Fukuju, T.; Yashiro, H.; Maeda, K.; Murai, H.; Azumi, T., *J. Phys. Chem. A* **1997**, *101*, 7783-7786.
7. Bortolus, M.; Prato, M.; van Tol, J.; Maniero, A. L., *Chem. Phys. Lett.* **2004**, *398*, 228-234.
8. Fuhs, M.; Elger, G.; Mobius, K.; Osintsev, A.; Popov, A.; Kurreck, H., *Mol. Phys.* **2000**, *98*, 1025-1040.
9. Tsuji, H.; Sasaki, M.; Shibano, Y.; Toganoh, M.; Kataoka, T.; Araki, Y.; Tamao, K.; Ito, O., *Bull. Chem. Soc. Jpn.* **2006**, *79*, 1338-1346.
10. Imahori, H.; Tkachenko, N. V.; Vehmanen, V.; Tamaki, K.; Lemmetyinen, H.; Sakata, Y.; Fukuzumi, S., *J. Phys. Chem. A* **2001**, *105*, 1750-1756.